UC Irvine
UC Irvine Previously Published Works

Title

Response to Çelikoyar re: "Video Standards for Rhinoplasty Education: A Review and Recommended Guidelines"

Permalink

Journal

ISSN

Authors

Hakimi, Amir A
Chen, Jason J
Wong, Brian JF

Publication Date

DOI

Copyright Information

Peer reviewed

Real-Time Subglottic Stenosis Imaging Using Optical Coherence Tomography in the Rabbit

Jennifer L. Lin, MD, **Amy Y. Yau, MD**, **Jonathon Boyd, MD**, **Ashley Hamamoto, BS**, **Erica Su, BS**, **Lauren Tracy, BS**, **Andrew E. Heidari, BS**, **Alex H. Wang, BS**, **Gurpreet Ahuja, MD**, **Zhongping Chen, MD**, and **Brian J. Wong, MD, PhD**
Beckman Laser Institute (Drs Lin, Yau, Boyd, Ahuja, Chen, Wong, Mss Hamamoto, Su, Tracey, Mssrs Heidari Wang), Departments of Otolaryngology–Head Neck Surgery (Drs Lin, Yau, Boyd, Ahuja, Wong) Biomedical Engineering (Mssrs Heidari Wang Drs Chen Wong), the Center for Biomedical Imaging (Mss Hamamoto, Su, Tracey Drs Chen Wong), University of California Irvine, Irvine; Children's Hospital of Orange County, Orange, California (Dr Ahuja)

Abstract

Importance—Subglottic stenosis (SGS) is a severe, acquired, potentially life-threatening disease that can be caused by endotracheal tube intubation. Newborns and neonates are particularly susceptible to SGS owing to the small caliber of their airway.

Objective—To demonstrate optical coherence tomography (OCT) capabilities in detecting injury and scar formation using a rabbit model. Optical coherence tomography may provide a noninvasive, bedside or intensive care unit modality for the identification of early airway trauma with the intention of preventing progression to SGS and can image the upper airway through an existing endotracheal tube coupled with a small fiber-optic probe.

Design—Rabbits underwent suspension laryngoscopy with induction of of SGS via epithelial injury. This model was used to test and develop our advanced, high-speed, high-resolution OCT imaging system using a 3-dimensional microelectromechanical systems-based scanning device integrated with a fiber-optic probe to acquire high-resolution anatomic images of the subglottic epithelium and lamina propria.

Setting—All experiments were performed at the Beckman Laser Institute animal operating room.

Intervention or Exposure—Optical coherence tomography and endoscopy was performed with suspension laryngoscopy at 6 different time intervals and compared with conventional digital endoscopic images and histologic sections. Fifteen rabbits were killed at 3, 7, 14, 21, and 42 days after the induction of SGS. The laryngotracheal complexes were serially sectioned for histologic analysis.

Main Outcome and Measure—Histologic sections, endoscopic images, and OCT images were compared with one another to determine if OCT could accurately delineate the degree of SGS achieved.

Results—The rabbit model was able to reliably and reproducibly achieve grade I SGS. The real-time OCT imaging system was able to (1) identify multiple structures in the airway; (2) delineate different tissue planes, such as the epithelium, basement membrane, lamina propria, and cartilage; and (3) detect changes in each tissue plane produced by trauma. Optical coherence tomography was also able demonstrate a clear picture of airway injury that correlated with the endoscopic and histologic images. With subjective review, 3 patients had high correlation between OCT and histologic images, 10 demonstrated some correlation with histologic images, and 2 showed little to no correlation with histologic images.

Conclusions and Relevance—Optical coherence tomography, coupled with a fiber-optic probe, identifies subglottic scarring and can detect tissue changes in the rabbit airway to a depth of 1 mm. This technology brings us 1 step closer to minimally invasive subglottic airway monitoring in the intubated neonate, with the ultimate goal of preventing SGS and better managing the airway.

Subglottic Stenosis is a Partial or complete circumferential narrowing of the airway, from either congenital malformation of the cricoid cartilage or acquired from injury to the delicate tissues that line the upper airway. Prior to 1935, most subglottic stenoses were caused by diphtheria and syphilis. Currently, 90% of acquired subglottic stenoses in children are caused by prolonged intubation.[1] Today, acquired subglottic stenosis occurs at an incidence of 0.63% of neonates intubated more than 48 hours, and it is most commonly caused by pressure necrosis from an endotracheal tube.[2] In neonates, stenosis occurs most commonly at the subglottis, the narrowest portion of the airway at this age. The site is also more prone to injury because the cricoid is a complete ring and cannot expand or flex in response to deformation. With high endotracheal pressures, 100% of the epithelium is lost in the first few hours, with major damage and ulceration occurring in the first 7 days.[3] Currently, subglottic stenosis is definitively diagnosed by performing surgical endoscopy following extubation failure or for workup of persistent stridor. Surgical endoscopy carries modest associated risk in this age group related to airway instrumentation and general anesthesia.[4-8]

Optical coherence tomography (OCT) is a noninvasive imaging modality that uses a low-coherence light source combined with a Michelson interferometer to produce high-resolution images (approximately 5-10 um) of tissues in cross-section.[9] Just as ultrasonography uses the acoustic properties of tissues, OCT relies on the tissues' optical properties to produce real-time imaging of living structures. The resolution allows for differentiation of layered tissue structures, such as the retina, skin, and mucosa. When coupled with a fiber-optic probe, it can image the neonatal airway through a preexisting endotracheal tube. Optical coherence tomography technology is rapidly expanding, with numerous possible clinical applications in the field of otolaryngology.[10-29]

The current investigation aims to further define the use of OCT technology to optimize neonatal intensive care unit (NICU)-based imaging of the neonatal airway. To accomplish this, a rabbit model of subglottic stenosis was adapted to this project for testing the OCT device and probe. To enable transition to imaging in the NICU, the probe must be optimized

for flexibility and a form factor to be introduced through an existing neonatal endotracheal tube. Airway anatomy seen with OCT also must be correlated with endoscopic imaging as well as histologic findings. Unlike earlier human patient studies published by our group, this study used a highspeed Fourier domain OCT system several orders of magnitude faster than previous time domain systems to generate real-time cross-sectional images that could also be viewed using after processing techniques, such as volumetric renderings.[13,15]

Method

Oct Device and Instrumentation

The OCT system is schematically illustrated in Figure 1. Light is generated from a near-infrared, high-speed sweeping laser (sweeping speed, 50 kHz; full width at half-maximum $\Delta\lambda = 100$ nm, 1310 nm [SS-OCT imaging system; Axsun Technology). The microelectromechanical systems (MEMs)-based laser source has a high coherence length (12 mm) and high power (20 mW on average). The beam is directed into a 1×2 10:90 coupler, with 90% power in the sample arm and 10% in the reference arm. The back-reflected signal from the reference arm and the backscattered signal from the sample arm are guided into a 2×2 coupler. The interference signals out of the 2×2 coupler are sent into a balanced amplified photodetector (PDB130C; Thorlabs Inc). A high-speed digitizer (ATS9350; AlazarTech) was used to digitize the resulting radiofrequency output from the photodetector. The resultant axial resolution of the SS-OCT system used in this study is approximately 8 μm, while the lateral resolution (diffraction limited) approaches 10 μm. The system acquires cross-sectional tomographic images at a frame rate of 41.66 per second, with each frame separated by 6.25 μm from one another. This separation distance can be modified as the pullback rate of the probe is controlled by a linear servomotor by which speed can be adjusted to suit the purpose or application.

The imaging probe consists of single-mode fiber, with a gradient refractive index (GRIN) lens attached at its distal end, a microrotational motor with reflective surface mounted on a spinning shaft, and a linear motorized translational stage. The GRIN lens is 1 mm in diameter and has a working distance of 5 mm. A glass tube is fused to the micromotor (Namiki Precision Jewel Co) and is placed in front of the GRIN lens to reflect the light toward the tissue as it rotates, resulting in a circumferential scan. The fiber and the GRIN lens are held together with a glass tube, and the micromotor are both packaged inside a plastic sheath, with the distal end sealed. The final packaged probe's outer diameter is 2.2 mm. The probe is attached on a linear motorized stage (Zaber Technologies Inc), and the stage is synchronously controlled by the computer, along with the image acquisition. To image the rabbit subglottis, the probe is placed inside the rabbit's airway at the desired location, and the linear translation stage gradually withdraws the probe at a speed of 0.25 mm per second with retrograde acquisition of images. With this setup, an axial 360° view of the airway can be obtained. With each pullback, hundreds of images are obtained sequentially from inferior to superior views.

Rabbit Subglottic Stenosis Model

Fifteen New Zealand white rabbits, ranging in weight from 3.5 to 4.2 kg, were used during the preliminary stage of our study. This study was performed under the aegis of the University of California institutional animal care and use committee. The rabbits were housed in an approved animal care facility with water and food ad libitum. The New Zealand white rabbit has been used in many subglottic studies and has been found to be a reliable model with different methods of airway scarring.[30-32] Rabbit subglottis dimensions (5.8×5.4 mm) at this weight range have been shown to correlate closely with those of a neonate (4.5-5.5 mm).[33] The rabbits were randomly assigned to 5 groups, each with a

different end point. Rabbits were anesthetized with subcutaneous injections of 2 mL of ketamine hydrochloride (35 mg/kg) and 1 mL of xylazine hydrochloride (5 mg/kg). Once anesthetized, the hair from one foreleg was clipped, and a pulse oximeter and heart rate monitor were attached to the leg. The rabbit was then placed supine on the operating table, and the glottis was exposed using a pediatric laryngoscope. 0.1 mL of 1% lidocaine was used topically to anesthetize the vocal cords. The airway was placed into suspension. A 0° Hopkins endoscope (Karl Storz GmbH & Co) was then placed through a 26 cm, size 3 bronchoscope (Karl Storz GmbH & Co) for photo-micrographic documentation of the native airway. To standardize the region of airway imaged by OCT, the tip of the bronchoscope was then positioned immediately below the vocal cords and secured in place by taping it to the laryngoscope. The OCT probe was then inserted into the bronchoscope to image the subglottic region starting exactly 2.5 cm past the distal end of the bronchoscope. A 2.5-cm region of the trachea and subglottis was sampled sequentially at 6.25-μm intervals with each pull-back of the probe, yielding 400 images, and a 3-dimensional image stack was generated. Pullback speed was fixed by attaching the probe to a stand mounted on a motor with adjustable speed. Epithelial injury in the subglottis was induced by introducing a nylon brush (a 16-in twisted wire nylon brush with a 5-mm diameter; Sharn MED) through the bronchoscope and rotating an average of 40 times along the surface. The working end of the brush was trimmed to 1 cm so that the epithelial damage could be restricted to a small controlled region. The rabbit was then taken out of suspension, recovered from anesthesia, and returned to the vivarium.

On subsequent study days, the rabbits were sedated and then resuspended for endoscopic and OCT image acquisition. The rabbits were killed 3, 7, 14, 21, or 42 days after initial airway injury to coincide with different stages of wound healing (Table). We had no unexpected early mortalities from this study, and all animals were killed on the date planned. Stridor was noted in only 1 rabbit in the first few days after induction of airway injury. The rabbits were killed after induction of anesthesia with an intravenous injection of 2 mL of pentobarbital sodium and phenytoin sodium (Euthasol; Virbac AH Inc). The laryngotracheal complex was then dissected and fixed in formaldehyde for histologic evaluation. After 24 hours in formaldehyde, samples were embedded in paraffin. The samples were serially sectioned into 6-μm annular thick slices and stained with hematoxylin-eosin. Photomicrographs (PictureFrame) were then taken for documentation.

Data Analysis

Serial sections of histologic specimens were examined at both low- and high-power magnification. The presence of inflammatory cells, fibroblasts, neovascularization, and reepithelialization was documented and corresponded with the course of normal tissue healing as expected, depending on the number of days after airway injury that the animals were sacrificed. A representative slice at the level of greatest airway scarring was selected.

To compare OCT with conventional histologic images, OCT images acquired on the day the animal was killed were compared with corresponding histologic sections of that rabbit's airway. Registration of the site of OCT image acquisition was achieved by identifying natural landmarks, such as the tip of the arytenoid cartilage, the cricoid cartilage, and the first tracheal ring. Registration of OCT with histologic images using markers in the airway is a challenge. In pilot studies, an initial group of rabbits had various materials injected into the sub-mucosa with fine-gauge spinal needles in an attempt to create a registry point to facilitate slice-by-slice comparison of OCT and histologic images. Contrast agents evaluated included india ink (standard tattoo ink), titanium dioxide, and colloidial gold. Although the material could be visually identified by endoscopy at the time of injection, subsequent endoscopic examination at later days failed to demonstrate persistent of the marker within

the tissues. These contrast agents were also not visualized during OCT imaging or later histologic section.

Selected paired OCT images and histologic sections were then presented to investigators at our institution with expertise in both OCT imaging and histology (A.Y.Y., J.B., E.S., A.H., A.E.H., B.J.W., and 2 investigators with expertise in OCT but not part of current study team). They were first asked to assess for the presence of airway scarring, then asked to rate the anatomic similarities between the OCT and histologic images. Grading was performed using a Likert scale where a score of 1 implied high correlation; 2, some correlation; and 3, little to no correlation. Other members of the study team were asked to trace the area of tissue thickening and the circumference of the native airway on hard copies with a marking pen. These drawings overlaid on OCT images were then scanned and the area calculated using Adobe Photoshop (Adobe Systems Inc). The scar area was then divided by the native airway area, and a percentage of airway occluded by scarring was thus estimated.

Result

Our method of inducing subglottic injury in the rabbit yielded consistent, reproducible results under multiple operators. Airway scarring measured by fractional airway area measurements ranged from 9% to 34% as identified by OCT, and 23% to 43% by histologic images. Airway scar area analysis results are shown in Figure 2. All 15 rabbits did have some degree of airway scarring, as confirmed by histologic images. Histologic changes were examined at each of the different time points after mucosal injury, and tissue changes were found to correlate well with known, normal wound healing.

Areas of overt scar or inflammation as seen on endoscopy were readily identified on the OCT images by examiners (J.L.L. and A.Y.Y.) during real-time acquisition. More subtle submucosal changes not identified during real-time image acquisition were noted in offline analysis when examining the images frame by frame using visualization or rendering software such as Quicktime (Apple Computer), Amira (Visage Imaging), or Mimics (Materialise). These changes were often not identified on endoscopy alone, and OCT imaging was found to be more sensitive than endoscopy in detecting subtle airway scarring and submucosal changes. This is to be expected, as OCT provides images in depth. Figure 3 demonstrates that the level of the airway can be gauged based on expected cartilage shape. Granulation tissue, as seen in endoscopic images, OCT, and histologic images in Figure 4, was the most obvious phase of wound healing to be picked up by OCT. With these early inflammatory changes there is a clear demarcation to normal epithelium. The lack of scar contracture and reepithelialization as seen in later stages of wound healing also make surface changes easy to visualize with OCT. Figure 5 demonstrates another stage of wound healing in which reepithelization and collagen formation are occurring, with submucosal changes that are clearly different on OCT than inflammation alone. Figure 6 and Figure 7 show the later stages of wound healing in which remodeling is occurring. Both figures demonstrate that OCT can detect both surface and submucosal changes along with correlative histologic images. The use of OCT to gauge the presence of scar formation using a simple 3-point scale provided interesting results. Of the 15 animals, all but 1 had evidence of scarring identified on OCT. Three animals had high correlation between OCT and histologic images, 10 demonstrated some correlation to histologic images, and 2 showed little or no correlation with histologic images. The 2 OCT images that reviewers overall thought had little to no correlation to histologic images had a large segment of the scarred tissue region blocked by the motor wire artifact. The scanning head of the OCT probe is a MEM's micromotor, and a wire by necessity delivers power, blocks the optical pathway, and obscures a full 360° view. Future technical developments may involve the development of external rotation systems as used by our group in other studies of the upper airway.[34-36]

Discussion

The long-term objective of our research is to develop OCT imaging systems that can be used in the NICU to image the microstructure of the neonatal subglottic airway with the intention of identifying early airway edema or trauma that might have the potential to progress to irreversible airway damage. Our ultimate goal is to better identify patients at risk for major airway injury from endotracheal intubation, provide additional structural information to enhance extubation criteria, and reduce the incidence of subglottic stenosis. Previous work by our group has demonstrated the feasibility of this approach in neonates and pediatric patients using slow, 2-dimensional time-domain OCT systems.[13,15]

This study represents the evolution and the technology aimed at refining OCT imaging technology for use in high-speed, high-resolution, real-time imaging of the neonatal intubated airway. The current work represents a move to high-speed Fourier domain technology. We have a reproducible rabbit model of subglottic stenosis and have shown the ability to detect phases of wound healing using OCT coupled with a fiber-optic probe in a suspended airway. Changes to the airway surface anatomy are easily identified by OCT and correlate with histologic findings. However, OCT performed using existing technology offers limited depth of optical penetration in turbid media; currently achievable depth of penetration is less than 1 mm. With thick scars or tissue swelling, the border between soft tissue and cartilage is not always visualized. Hence, extensive local soft-tissue injury, swelling, and scar with associated major increases in tissue thickness can pose a challenge.

Regardless of the limited information at deeper tissue levels, examiners who compared OCT and histologic images were able to identify areas of airway stenosis in both data sets. Among OCT experts, the area of stenosis was consistently identified within a standard error of 2.8%, and among histology experts, the area of stenosis was consistently identified within a standard error of 3.2%. However, between OCT and histologic images, there was general trend in reporting lower-than-expected degrees of airway stenosis in the OCT group. This can be accounted for in several ways. First, the shadow cast by the MEMs motor wire eliminated signal from a region of interest, and in that area tissue was simply not evaluated on OCT. Second, the limited depth of tissue penetration by the current OCT system may not have measured the full thickness of the scar. Third, the current probe's working distance was unable to capture the entire airway in a 360° manner in wider cross-sectional areas of the airway, and fourth, compression artifact and warping of the specimens during histologic preparation led to flattening of the specimens, thereby effectively decreasing the measured airway area. We are working on addressing these issues in future studies, and we are building a long-range OCT system to be able to capture images over greater distances.

Fourier domain long-range OCT systems have only recently become an area of interest for optical engineers and scientists.[37] It is a focus of our research group as well. Depth of penetration remains a vexing issue for all OCT systems because optical scattering and absorption limit the return of coherent photomicrographs to the imaging system. Typically, 0.5 to 1.0 mm is the depth of penetration at which useable information can be obtained, but this varies immensely with tissue turbidity, the presence of blood, or scattering media (eg, turbid secretions, refluxed gastric contents). This is a fundamental limitation of this technology.

We posit that OCT has the potential to determine the maturity of the scar based on texture analysis and segmentation of signals, as well as volumetric rendering. Recent trauma will have more edema and fluid, and a mature scar will have more collagen. Collagen is turbid, scatters light, and would increase the signal intensity, albeit at the expense of reduced signal from deeper tissue layers. Detailed analysis (segmentation and texture) should be able to

characterize the turbidity of the tissue and thereby effectively determine the maturity of the scar. Grayscale analysis is used widely in medical imaging but is challenging to implement in low-contrast imaging methods, such as OCT. This is a challenge common to imaging methods, such as ultrasonography and magnetic resonance imaging. Segmentation and automated image analysis, which are beyond the scope of this work, will allow for a more detailed evaluation of the OCT images and better define the relationship between scar tissue seen on histologic images. Simple comparison of grayscale intensity alone is challenging given image artifacts in histologic sections and the lack of normalization of contrast and brightness of the OCT source. Subjective analysis of OCT imaging was quite variable depending on the skill and experience of the persons reading the images. Like ultrasonography, there is definitely a learning curve. Also like ultrasonography, viewing a temporal sequence of images (a "movie") often provides a better sense of tissue structure than just an isolated still image. We hope to further refine the probe and develop better measurement techniques involving image analysis– and segmentation-driven methods.

Current and future ongoing research is focused on using the present rabbit model to study subglottic and tracheal edema. Edema is perhaps more important than scar formation because it is a possible sign of early airway injury. This will further allow us to characterize the ability of OCT imaging to identify changes in the submucosa with the goal of routine airway monitoring in the NICU.

In conclusion, endotracheal tube intubation is a life-saving intervention, but it does come with risks. Otolaryngologists are much too familiar with intubation-induced acquired subglottic stenosis in neonates. Severe subglottic stenosis can be a considerable challenging problem to address, with potential grave sequelae. Optical coherence tomography is a noninvasive imaging technique, which, we believe, can be successfully applied to imaging the airway through a preexisting endotracheal tube. Our long-term goal is to apply OCT imaging at the bedside in intubated neonates. If we can image the microstructure of the neonatal subglottic airway and identify airway edema or early trauma, this may allow for changes in airway management that might avert irreversible airway damage.

Acknowledgments

References

1. Santos D, Mitchell R. The history of pediatric airway reconstruction. Laryngoscope. 2010; 120(4): 815–820. [PubMed: 20205174]

2. Choi SS, Zalzal GH. Changing trends in neonatal subglottic stenosis. Otolaryngol Head Neck Surg. 2000; 122(1):61–63. [PubMed: 10629484]

3. Hawkins DB. Hyaline membrane disease of the neonate prolonged intubation in management: effects on the larynx. Laryngoscope. 1978; 88(2, pt 1):201–224. [PubMed: 621987]

4. Bailey CM. Surgical management of acquired subglottic stenosis. J Laryngol Otol Suppl. 1988; 17:45–48. [PubMed: 3199001]

5. Contencin P, Narcy P. Study Group for Neonatology and Pediatric Emergencies in the Parisian Area. Size of endotracheal tube and neonatal acquired subglottic stenosis. Arch Otolaryngol Head Neck Surg. 1993; 119(8):815–819. [PubMed: 8343241]

6. Dankle SK, Schuller DE, McClead RE. Risk factors for neonatal acquired sub-glottic stenosis. Ann Otol Rhinol Laryngol. 1986; 95(6, pt 1):626–630. [PubMed: 3789597]

7. Gould SJ, Graham JM. Acquired subglottic stenosis in neonates. Clin Otolaryngol Allied Sci. 1985; 10(6):299–302. [PubMed: 3830476]

8. Myer CM III. Diagnosis of acquired subglottic stenosis. J Pediatr. 1987; 110(1):163–164. [PubMed: 3794882]

9. Huang D, Swanson EA, Lin CP, et al. Optical coherence tomography. Science. 1991; 254(5035): 1178–1181. [PubMed: 1957169]

10. Kobler JB, Chang EW, Zeitels SM, Yun SH. Dynamic imaging of vocal fold oscillation with four-dimensional optical coherence tomography. Laryngoscope. 2010; 120(7):1354–1362. [PubMed: 20564724]

11. Klein AM, Pierce MC, Zeitels SM, et al. Imaging the human vocal folds in vivo with optical coherence tomography: a preliminary experience. Ann Otol Rhinol Laryngol. 2006; 115(4):277–284. [PubMed: 16676824]

12. Armstrong WB, Ridgway JM, Vokes DE, et al. Optical coherence tomography of laryngeal cancer. Laryngoscope. 2006; 116(7):1107–1113. [PubMed: 16826043]

13. Ridgway JM, Ahuja G, Guo S, et al. Imaging of the pediatric airway using optical coherence tomography. Laryngoscope. 2007; 117(12):2206–2212. [PubMed: 18322424]

14. Ridgway JM, Armstrong WB, Guo S, et al. In vivo optical coherence tomography of the human oral cavity and oropharynx. Arch Otolaryngol Head Neck Surg. 2006; 132(10):1074–1081. [PubMed: 17043254]

15. Ridgway JM, Su J, Wright R, et al. Optical coherence tomography of the newborn airway. Ann Otol Rhinol Laryngol. 2008; 117(5):327–334. [PubMed: 18564528]

16. Rubinstein M, Fine EL, Sepehr A, et al. Optical coherence tomography of the larynx using the Niris system. J Otolaryngol Head Neck Surg. 2010; 39(2):150–156. [PubMed: 20211101]

17. Rubinstein M, Schalch P, Di Silvio M, Betancourt MA, Wong BJ. Optical coherence tomography applications in otolaryngology. Acta Otorrinolaringol Esp. 2009; 60(5):357–363. [PubMed: 19814989]

18. Sepehr A, Armstrong WB, Guo S, et al. Optical coherence tomography of the larynx in the awake patient. Otolaryngol Head Neck Surg. 2008; 138(4):425–429. [PubMed: 18359348]

19. Sepehr A, Djalilian HR, Chang JE, Chen Z, Wong BJ. Optical coherence tomography of the cochlea in the porcine model. Laryngoscope. 2008; 118(8):1449–1451. [PubMed: 18496151]

20. Wong BJ, Jackson RP, Guo S, et al. In vivo optical coherence tomography of the human larynx: normative and benign pathology in 82 patients. Laryngoscope. 2005; 115(11):1904–1911. [PubMed: 16319597]

21. Yu L, Liu G, Rubinstein M, Saidi A, Wong BJ, Chen Z. Office-based dynamic imaging of vocal cords in awake patients with swept-source optical coherence tomography. J Biomed Opt. 2009; 14(6):064020. [PubMed: 20059258]

22. Burns JA, Kim KH, deBoer JF, Anderson RR, Zeitels SM. Polarization-sensitive optical coherence tomography imaging of benign and malignant laryngeal lesions: an in vivo study. Otolaryngol Head Neck Surg. 2011; 145(1):91–99. [PubMed: 21493273]

23. Burns JA, Zeitels SM, Anderson RR, Kobler JB, Pierce MC, de Boer JF. Imaging the mucosa of the human vocal fold with optical coherence tomography. Ann Otol Rhinol Laryngol. 2005; 114(9):671–676. [PubMed: 16240928]

24. Burns JA, Kim KH, Kobler JB, deBoer JF, Lopez-Guerra G, Zeitels SM. Real-time tracking of vocal fold injections with optical coherence tomography. Laryngoscope. 2009; 119(11):2182–2186. [PubMed: 19676103]

25. Jerjes W, Upile T, Conn B, et al. In vitro examination of suspicious oral lesions using optical coherence tomography. Br J Oral Maxillofac Surg. 2010; 48(1):18–25. [PubMed: 19726114]

26. Kraft M, Glanz H, Gerlach Sv, Wisweh H, Lubatschowski H, Arens C. Morphologic classification of Reinke's edema through optical coherence tomography. Laryngorhinootologie. 2010; 89(4):224–227. [PubMed: 19998217]

27. Kraft M, Glanz H, von Gerlach S, Wisweh H, Lubatschowski H, Arens C. Optical coherence tomography: significance of a new method for assessing unclear laryngeal pathologies. HNO. 2010; 58(5):472–479. [PubMed: 19145422]

28. Kraft M, Lüerssen K, Lubatschowski H, Glanz H, Arens C. Technique of optical coherence tomography of the larynx during microlaryngoscopy. Laryngoscope. 2007; 117(5):950–952. [PubMed: 17473703]

29. Kraft M, Glanz H, von Gerlach S, Wisweh H, Lubatschowski H, Arens C. Clinical value of optical coherence tomography in laryngology. Head Neck. 2008; 30(12):1628–1635. [PubMed: 18767182]

30. Steehler MK, Hesham HN, Wycherly BJ, Burke KM, Malekzadeh S. Induction of tracheal stenosis in a rabbit model-endoscopic versus open technique. Laryngoscope. 2011; 121(3):509–514. [PubMed: 21344426]

31. Nakagishi Y, Morimoto Y, Fujita M, Ozeki Y, Maehara T, Kikuchi M. Rabbit model of airway stenosis induced by scraping of the tracheal mucosa. Laryngoscope. 2005; 115(6):1087–1092. [PubMed: 15933527]

32. Roh JL, Lee YW, Park HT. Subglottic wound healing in a new rabbit model of acquired subglottic stenosis. Ann Otol Rhinol Laryngol. 2006; 115(8):611–616. [PubMed: 16944660]

33. Loewen MS, Walner DL. Dimensions of rabbit subglottis and trachea. Lab Anim. 2001; 35(3): 253–256. [PubMed: 11459410]

34. Lee SW, Heidary AE, Yoon D, et al. Quantification of airway thickness changes in smoke-inhalation injury using in-vivo 3-D endoscopic frequency-domain optical coherence tomography. Biomed Opt Express. 2011; 2(2):243–254. [PubMed: 21339870]

35. Zhang J, Jing J, Wang P, Chen Z. Polarization-maintaining buffered Fourier domain mode-locked swept source for optical coherence tomography. Opt Lett. 2011; 36(24):4788–4790. [PubMed: 22179884]

36. Yin J, Li X, Jing J, et al. Novel combined miniature optical coherence tomography ultrasound probe for in vivo intravascular imaging. J Biomed Opt. 2011; 16(6):060505. [PubMed: 21721799]

37. Wang L, Dixit L, Weikert MP, Jenkins RB, Koch DD. Healing changes in clear corneal cataract incisions evaluated using Fourier-domain optical coherence tomography. J Cataract Refract Surg. 2012; 38(4):660–665. [PubMed: 22321355]
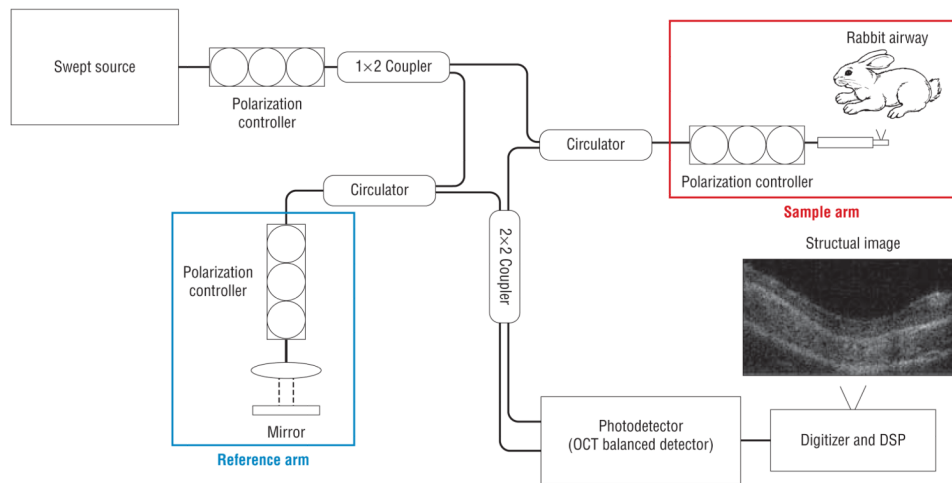
Figure 1.
Schematics of the optical coherence tomography system built by University of California, Irvine, department of biomedical engineering in conjunction with Beckman Laser Institute used in this current rabbit model. DSP indicates digital signal processing; OCT, optical coherence tomography.
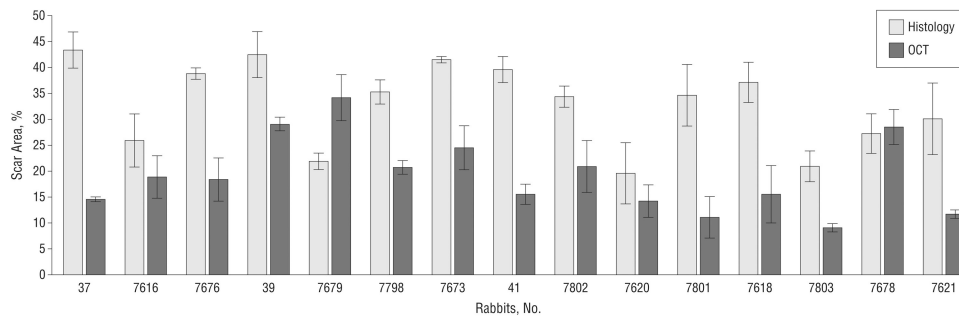
Figure 2.
The area of scar as seen by optical coherence tomography (OCT) and histologic examination was evaluated by blinded investigators. The x-axis shows the rabbit numbers. Airway scarring measured by fractional airway area measurements ranged from 9% to 34% as identified by OCT, and 23% to 43% by histologic images. Among OCT experts, the area of stenosis was consistently identified within a standard error of 2.8%, and among histology experts, the area of stenosis was consistently identified within a standard error of 3.2%. Error bars indicate standard errors.
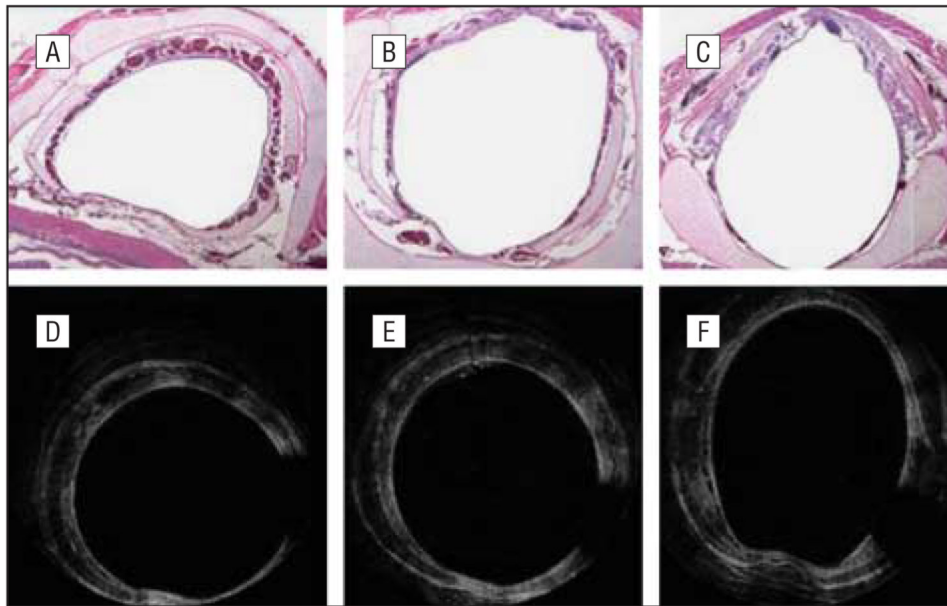
Figure 3.
Histologic images (A-C) and optical coherence tomographic (OCT) images (D-F) of a control rabbit. A, An axial slice of the airway at the most inferior edge of the cricoid cartilage and the first tracheal ring. B, The cricoid cartilage. C, The most superior aspect of the cricoid cartilage. D-F, The level of the airway can be gauged based on the shape change of the airway as demonstrated by these figures. The classic sideways "D" is seen with the tracheal rings, a circular shape at the level of the cricoid and the ovoid shape at the immediate subglottic. The missing data at the 5-o'clock position are a shadow caused by the motor wire of the OCT probe.
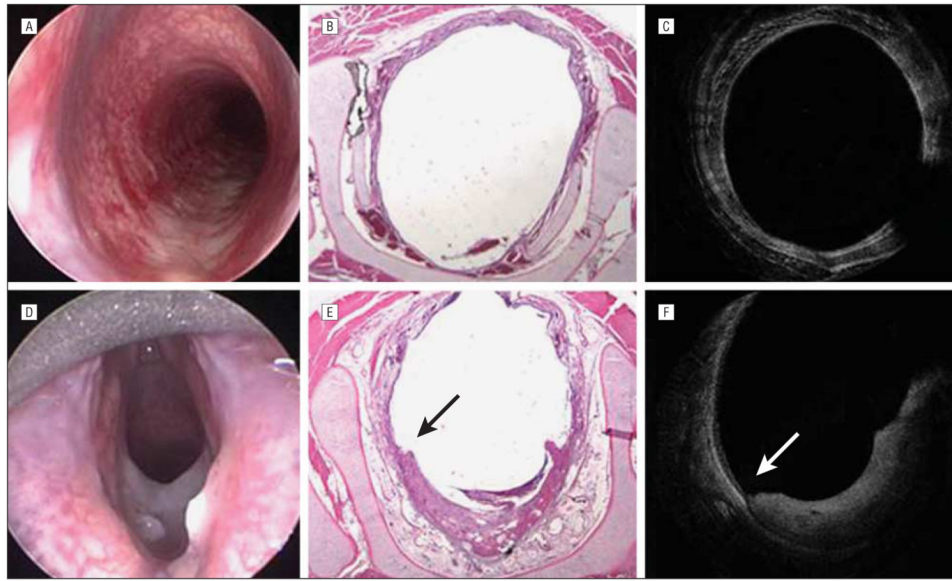
Figure 4.
Images of the subglottic region of rabbits studied. Endoscopic (A), histologic (B), and optical coherence tomographic (OCT) (C) images of the subglottic region of a control rabbit. Endoscopic (D), histologic (E), and OCT (F) images of the subglottic region of a rabbit 3 days after mucosal injury. In all 3 images, there is a clear area of mucosal abnormality from the 4-o'clock to 8-o'clock positions, with a clear demarcation between intact epithelium and damaged epithelium. Histologic images confirm the presence of granulation tissue, early blood vessel formation, hemorrhage, and abundant lymphocytes. The arrows point to a clear area of demarcation for normal epithelium and damaged epithelium
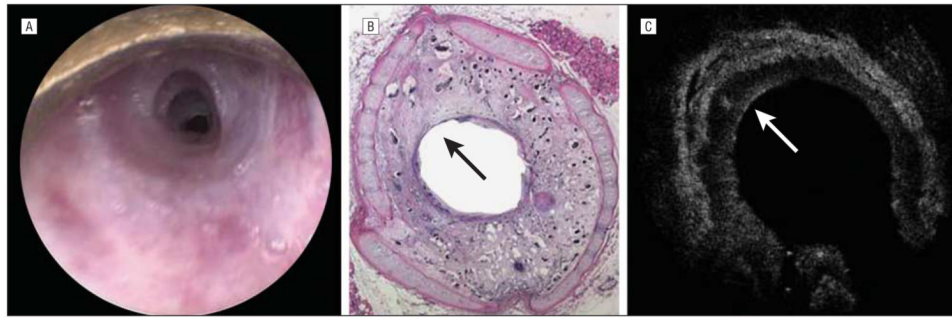
Figure 5.
A rabbit killed 14 days after mucosal injury. A scar on endoscopy (A), a scar on histologic images (B), and a scar on optical coherence tomography (OCT) (C) images. All 3 modalities show significant circumferential scarring in the airway. On OCT, the tissue penetration is limited, and therefore the entire thickness of the scar is not visualized; however, clear evidence of reepitheliazation is seen at the 11-o'clock position as indicated by the arrows and correlates with histology. Submucosal tissue injury is evident.
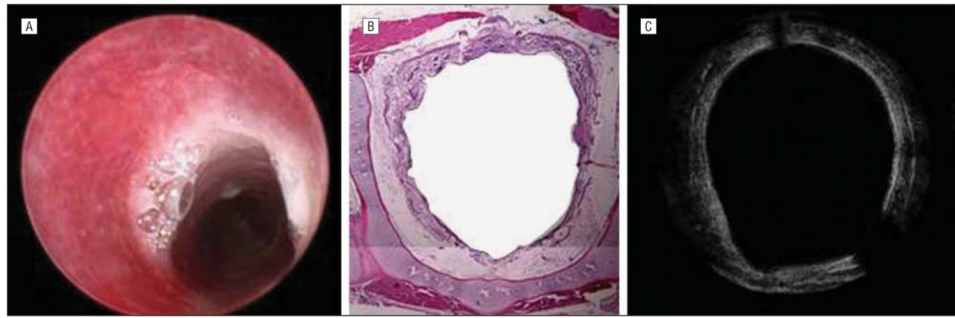
Figure 6.
A rabbit killed 21 days after mucosal injury. Endoscopic (A), histologic (B), and optical coherence tomographic (C) images. Circumferential scarring with reepithelialization are seen in all imaging modalities.
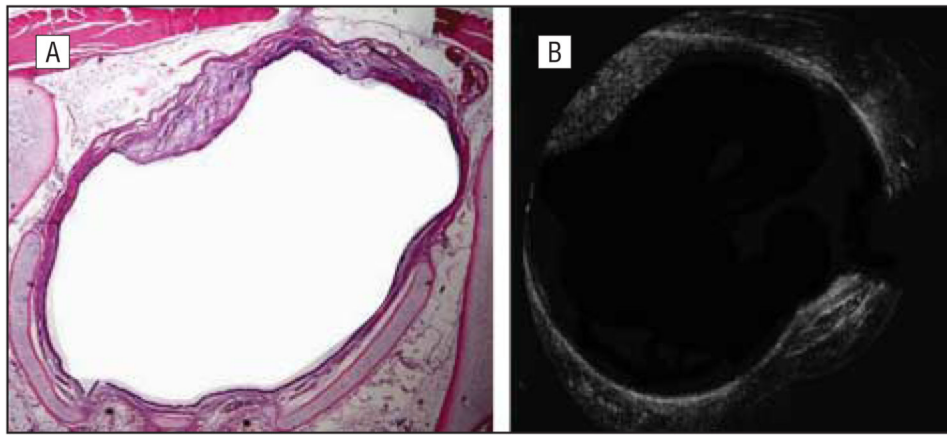
Figure 7.
A rabbit killed 42 days after mucosal injury. Histologic (A) and optical coherence tomographic (OCT) (B) images show a single area of fibrous scarring at the 11-o'clock position. The OCT image very clearly demonstrates changes in both surface and submucosal anatomy that correlates well with histologic images.

Table

Experimental Design

Arm	0	3	7	14	21	42
			Post-Brush Injury Day[a]			
1	Endoscopy OCT Brush injury	Endoscopy OCT Rabbit is killed	…	…	…	…
2	Endoscopy OCT Brush injury	Endoscopy OCT	Endoscopy OCT Rabbit is killed	…	…	…
3	Endoscopy OCT Brush injury	…	Endoscopy OCT	Endoscopy OCT Rabbit is killed	…	…
4	Endoscopy OCT Brush injury	…	Endoscopy OCT	Endoscopy OCT	Endoscopy OCT Rabbit is killed	…
5	Endoscopy OCT Brush injury	…	…	Endoscopy OCT	Endoscopy OCT[b]	Endoscopy OCT Rabbit is killed

Abbreviation: OCT, optical coherence tomography.

[a]Rabbits underwent suspension laryngoscopy with induction of epithelial injury using a stiff-bristled brush, which led to the development of subglottic stenosis. Endoscopy and OCT imaging were performed on rabbits in days 0, 3, 7, 14, 21, and 42. Histologic images correlate with the day that the rabbit was killed.

[b]Rabbits in this arm were also imaged with endoscopy and OCT on post–brush injury day 35.